An Ionizing Radiation Acoustic Imaging (iRAI) Technique for Real-Time Dosimetric Measurements for FLASH Radiotherapy

Ibrahim Oraiqat[†*]
Department of Radiation Oncology, University of Michigan, Ann Arbor, Michigan 48109, USA
Wei Zhang[†]
Department of Biomedical Engineering, University of Michigan, Ann Arbor, Michigan 48109, USA
Dale Litzenberg
Department of Radiation Oncology, University of Michigan, Ann Arbor, Michigan 48109, USA
Kwok Lam
Department of Radiation Oncology, University of Michigan, Ann Arbor, Michigan 48109, USA
Noora Ba Sunbul
Department of Nuclear Engineering, University of Michigan, Ann Arbor, Michigan 48109, USA
Jean Moran
Department of Radiation Oncology, University of Michigan, Ann Arbor, Michigan 48109, USA
Kyle Cuneo
Department of Radiation Oncology, University of Michigan, Ann Arbor, Michigan 48109, USA
Paul Carson
Department of Radiology, University of Michigan, Ann Arbor, Michigan 48109, USA
Xueding Wang
Department of Biomedical Engineering, University of Michigan, Ann Arbor, Michigan 48109, USA
Department of Radiology, University of Michigan, Ann Arbor, Michigan 48109, USA
Issam El Naqa
Department of Radiation Oncology, University of Michigan, Ann Arbor, Michigan 48109, USA

† These authors contributed equally to this work.

**Corresponding author:* ioraiqat@umich.edu

This is the author manuscript accepted for publication and has undergone full peer review but has not been through the copyediting, typesetting, pagination and proofreading process, which may lead to differences between this version and the Version of Record. Please cite this article as doi: 10.1002/MP.14358

An Ionizing Radiation Acoustic Imaging (iRAI) Technique for Real-Time Dosimetric Measurements for FLASH Radiotherapy

Ibrahim Oraiqat[†*]
Department of Radiation Oncology, University of Michigan, Ann Arbor, Michigan 48109, USA
Wei Zhang[†]
Department of Biomedical Engineering, University of Michigan, Ann Arbor, Michigan 48109, USA
Dale Litzenberg
Department of Radiation Oncology, University of Michigan, Ann Arbor, Michigan 48109, USA
Kwok Lam
Department of Radiation Oncology, University of Michigan, Ann Arbor, Michigan 48109, USA
Noora Ba Sunbul
Department of Nuclear Engineering, University of Michigan, Ann Arbor, Michigan 48109, USA
Jean Moran
Department of Radiation Oncology, University of Michigan, Ann Arbor, Michigan 48109, USA
Kyle Cuneo
Department of Radiation Oncology, University of Michigan, Ann Arbor, Michigan 48109, USA
Paul Carson
Department of Radiology, University of Michigan, Ann Arbor, Michigan 48109, USA
Xueding Wang
Department of Biomedical Engineering, University of Michigan, Ann Arbor, Michigan 48109, USA
Department of Radiology, University of Michigan, Ann Arbor, Michigan 48109, USA
Issam El Naqa
Department of Radiation Oncology, University of Michigan, Ann Arbor, Michigan 48109, USA

† *These authors co*ntributed equally to this work.

*Corresponding author: ioraiqat@umich.edu

Purpose: FLASH radiotherapy (FLASH-RT) is a novel irradiation modality with ultra-high dose rates (>40Gy/s) that have shown tremendous promise for its ability to enhance normal tissue sparing while maintaining comparable tumor cell eradication to conventional radiotherapy (CONV-RT). Due to its extremely high-dose rates, clinical translation of FLASH-RT is hampered by risky delivery and current limitations in dosimetric devices, which cannot accurately measure, in real-time, dose at deeper tissue. This

work aims to investigate ionizing radiation acoustic imaging (iRAI) as a promising image-guidance modality for real-time deep tissue dose measurements during FLASH-RT. The underlying hypothesis is that iRAI can enable mapping of dose deposition with respect to surrounding tissue with a single linear accelerator (linac) pulse precision in real time. In this work, the relationship between iRAI signal response and deposited dose was investigated as well as the feasibility of using a proof-of-concept dual-modality imaging system of ultrasound and iRAI for treatment beam co-localization with respect to underlying anatomy.

Methods: Two experimental setups were used to study the feasibility of iRAI for FLASH-RT using 6 MeV electrons from a modified Varian Clinac. First, experiments were conducted using a single element focused transducer to take a series of point measurements in a gelatin phantom, which was compared with independent dose measurements using GAFchromic film. Secondly, an ultrasound and iRAI dual-modality imaging system utilizing a phased array transducer was used to take co-registered 2D iRAI signal amplitude images as well as ultrasound B-mode images, to map the dose deposition with respect to surrounding anatomy in an ex-vivo rabbit liver model with a single linac pulse precision.

Results: Using a single element transducer, iRAI measurements showed a highly linear relationship between the iRAI signal amplitude and the linac dose per pulse ($r^2 = 0.9998$) with a repeatability precision of 1% and a dose resolution error less than 2.5% in a homogenous phantom when compared to GAFchromic film dose measurements. These phantom results were used to develop a calibration curve between the iRAI signal response and the delivered dose per pulse. Subsequently, a normalized depth dose curve was generated that agreed with film measurements with an RMSE of 0.0243, using correction factors to account for deviations in measurement conditions with respect to calibration. Experiments on the ex-vivo rabbit liver model demonstrated that a 2D iRAI image could be generated successfully from a single linac pulse, which was fused with the B-mode ultrasound image to provide information about the beam position with respect to surrounding anatomy in real time.

Conclusion: This work demonstrates the potential of using iRAI for real-time deep tissue dosimetry in FLASH-RT. Our results show that iRAI signals are linear with dose and can accurately map the delivered radiation dose with respect to soft tissue anatomy. With its ability to measure dose for individual linac pulses at any location within surrounding soft tissue while identifying where that dose is being delivered anatomically in real time, iRAI can be an indispensable tool to enable safe and efficient clinical translation of FLASH-RT.

Index Terms— FLASH radiotherapy, medical imaging, radiation acoustics, in-vivo dosimetry, ultrasound

Introduction

A major goal of radiotherapy (RT) is to improve cancer eradication while minimizing complications to surrounding normal tissues. In a conventional radiotherapy (CONV-RT) setting, image-guidance techniques and virtual simulations during treatment planning are typically used to ensure that the planned irradiation beam delivered from a linear accelerator (linac) conforms to the targeted cancer area while minimizing dose exposure to surrounding normal tissues. However, several studies have highlighted discrepancies between planned and delivered radiation treatments and their impact on tumor eradication and surrounding normal tissue injury [1]. Unfortunately, these differences are exacerbated due to accumulative setup errors and organ motions over the course of fractionated radiotherapy treatment. This is particularly true for a novel irradiation modality, known as FLASH radiotherapy (FLASH-RT), where an ultra-high dose rate (>40 Gy/s) is being delivered almost instantaneously, which is orders of magnitude higher than conventional dose rates (~0.1 Gy/s) [2-5].

Interest in FLASH-RT has surged recently because of its unique ability to increase the differential effect between normal tissue and tumors, hence, improving the therapeutic ratio by at least 20-30% in preclinical studies. These encouraging results have been demonstrated in many in vivo systems. For example, it has been demonstrated in mice that irradiation under FLASH-RT conditions had reduced deleterious neurocognitive effects (deficits in learning and memory) compared with mice treated with conventional RT [2-5]. Additionally, studies with mice have also shown a significant reduction in lung fibrosis [6, 7]. Furthermore, the benefits of FLASH have been seen in higher mammals. Previous work with FLASH dose rates has shown that skin toxicities were reduced (no severe late skin fibronecrosis observed using FLASH, for example) in mini-pigs and toxicities (mucositis and depilation) were reduced in cats being treated for squamous cell carcinoma of the nasal planum [8]. Most recently, a clinical study was performed on a 75-year-old patient presented with cutaneous lymphoma [9]. The patient was treated successfully with a single 15 Gy FLASH-RT fraction in 90 milliseconds with minimal side effects, demonstrating the potential of FLASH-RT but also revealing its current clinical limitation as a surface-based RT only modality where safe irradiation with common techniques using established dosimetry is permissible. Applying the promise of FLASH-RT beyond surface irradiation, however, is hampered by the lack of proper dosimetric methods, which are able to accurately measure, in real-time, irradiation dose in deeper tissues to ensure safe delivery. Hence, there is a need to investigate new FLASH imaging technologies to address this challenge as presented in this work.

Typically, a clinical linac delivers radiation dose in a series of pulses. In CONV-RT, the dose per pulse is small (~0.05 cGy) with respect to the total dose typically used in treatment, allowing the mean dose rate to be measured by averaging dose over seconds or minutes. Due to the high dose per pulse used during FLASH-RT, only a handful of pulses would be used in each treatment, thus dose measurements on a pulse-to-pulse basis become essential, if not mandatory [10]. The gold standard for radiation beam characterization is ionization chambers (IC). Using ICs at the ultra-high FLASH dose rates can become problematic due to the reported decrease of ion collection efficiency with increased dose per pulse, requiring the use of an empirical model for additional correction factors [11]. For high dose rate dosimetry, film can be appropriate as it has been found to be dose rate independent [12] and can be placed directly on the surface of the patient. However, film is not a real-time measurement nor it can be used in vivo, thus it is better suited for quality assurance of the treatment plan rather than in vivo dosimetric measurement as would be needed for safe FLASH-RT delivery. It is important to point out that even though some current dosimetry methods can be used for FLASH-RT, they are limited to surface measurements and do not allow for any real time feedback, dose measurement in deeper tissue, or mapping the irradiated treatment volume for each linac pulse. For clinical translation of FLASH-RT, it will be highly valuable to quantify the deposited dose for individual linac pulses at the treatment volume at depth (as opposed to surface measurements only) as well to register this dose with the patient's anatomy irradiated to ensure that the dose is deposited accurately and safely at the intended target in real time.

Ionizing radiation acoustic imaging (iRAI) is an emerging medical imaging and real-time dosimetry modality that allows for such online in vivo deep tissue dosimetry [13, 14]. As ionizing radiation from the linac goes through tissue, it is attenuated, depositing energy. This absorbed energy, which is quantified as dose, in the targeted tissue will cause local, transient temperature rise in the irradiated volume. The heating causes a transient thermal expansion, which generates an initial pressure which propagates as acoustical waves, in what is known as the thermoacoustic effect [15, 16]. This elastic wave, containing information about the targeted tissue and radiation absorption, can be collected by ultrasound transducers located on the surface of the body around a region of interest. Since for a given tissue structure and beam geometry, the initial pressure is linearly proportional to the energy deposited (radiation dose), both the beam location and the dose deposition information can be extracted from the detected pressure wave. Therefore, we hypothesize here that, when iRAI is combined with ultrasound imaging (US), this dual-modality imaging will provide an effective way to guide FLASH-RT delivery safely, in vivo, in real time. Specifically, iRAI would allow for real-time imaging of dose deposition that can be inherently registered with the exposed tissue anatomy image from US [17, 18]. Several previous studies have demonstrated the feasibility of iRAI in providing clinically acceptable dosimetry from photons and electrons using either non-tomographic or tomographic (XACT) methods during external beam radiation therapy [15, 16, 19, 20], as well as some

early work on using the radiation acoustics generated from a pulsed proton beam to study the feasibility for non-invasive dose monitoring of a patient's liver [21]. However, the linearity of iRAI as a dosimetry tool under extremely high dose rates and the potential application of iRAI to guide FLASH-RT still haven't been explored.

In this work, and for the first time to the best of our knowledge, this novel dosimetry method, iRAI, is proposed for FLASH-RT allowing for deep tissue real-time dosimetry, which would constitute a major breakthrough towards safe clinical implementation of FLASH-RT. The feasibility of using iRAI for dosimetric measurements by investigating the relationship between the generated iRAI signal during delivery and the absorbed deposited dose, as well as real-time dose mapping tool using a proof-of-concept US and iRAI dual-modality imaging system, are evaluated via experiments in both phantoms and soft tissue samples during FLASH-RT.

Materials and Methods

Theory

In the processing of electron beam radiation therapy, the Linac-generated high energy electron beam impinged on the targeted tissue medium causing Coulomb interactions between the incident electrons and orbital electrons of the medium, resulting in ionizations of the medium atoms, or interaction with the nuclei of the medium atoms, resulting in electron scattering and energy loss of the electron through production of x-ray photons (bremsstrahlung). These energy losses are characterized by mass–energy stopping power (S/ρ), where S is the loss of the kinetic energy of the electron per unit length and ρ is the density of the medium. These losses determine the electrons' travel range. The ionization interactions contribute to the deposited dose during this pulse:

$$D_r(\mathrm{r},\mathrm{t}) = \emptyset(\mathrm{r},\mathrm{t})\left(\frac{\mathrm{S}}{\rho}\right)_{\mathrm{col}} \quad (1)$$

where $\emptyset$ is the number electrons per unit area (electron fluence) produced during a pulse. The "col" subscript refers to the collisional (ionization) part of the mass–energy stopping power. The local heat produced can then be given by:

$$H(\boldsymbol{r},t) = \eta_{th}\rho D_r(\boldsymbol{r},t) \quad (2)$$

where $H(\boldsymbol{r},t)$ is the heat absorption rate at location $\boldsymbol{r} \in \boldsymbol{R^3}$ and time t, and η_{th} is the thermal efficiency. The temperature rise distribution $T(\boldsymbol{r},t)$ due to $H(\boldsymbol{r},t)$ follows the heat transfer equation:

$$\rho C_v \frac{\partial T(\boldsymbol{r},t)}{\partial t} = \lambda \nabla^2 T(\boldsymbol{r},t) + H(\boldsymbol{r},t) \tag{3}$$

where C_v is specific heat capacity, and λ is the thermal conductivity. Following our previous approach [13], this can be rewritten as:

$$\frac{\partial T(\boldsymbol{r},t)}{\partial t} = \frac{\eta_{th} D_r(\boldsymbol{r},t)}{C_v} \tag{4}$$

Hence, the wave equation governing the generation and propagation of electron induced acoustic pressure is given by:

$$\left(\nabla^2 - \frac{1}{v_s^2}\frac{\partial^2}{\partial t^2}\right) p(\boldsymbol{r},t) = -\frac{\beta K_T \eta_{th}}{v_s^2 C_v}\frac{\partial D_r(\boldsymbol{r},t)}{\partial t} \tag{6}$$

where $v_s = \sqrt{K_T/\rho}$ is the speed of sound, β is the volumetric thermal expansion coefficient, and K_T is the isothermal bulk modulus. To match the frequency bandwidth of the radiation-induced acoustic signal, low frequency transducer probes were employed in this study. The temporal profile of each electron beam pulse can be represented as a Dirac delta function [13]. Hence, the iRAI pressure detected at the transducer position $\boldsymbol{r}$ and time t can be expressed by:

$$p(\boldsymbol{r},t) = \frac{1}{4\pi v_s^2}\int d\boldsymbol{r}' \frac{1}{|\boldsymbol{r}-\boldsymbol{r}'|}\Gamma \eta_{th}\rho D_p(\boldsymbol{r}')\delta\left(t - \frac{|\boldsymbol{r}-\boldsymbol{r}'|}{v_s}\right) \tag{7}$$

where $D_p(\boldsymbol{r}') = D_r(\boldsymbol{r},t)\cdot\tau_p$ is the deposited dose due to a signal electron beam pulse, τ_p is the pulse duration of electron beam. In the meantime, Γ is the Grüneisen parameter defined as:

$$\Gamma = \frac{\beta K_T}{C_v \rho} \tag{8}$$

This is a tissue specific parameter. It is noticed from Eq. 7 that the pressure wave is directly proportional to the Grüneisen parameter and the rate of change in the deposited dose. In the case of CONV-RT, this would be on the order of 0.05 cGy per pulse, which corresponds to an acoustic pressure on the order of 10 mPa. Measuring of such a small pressure would require a high gain signal amplification and substantial signal averaging to enhance the signal-to-noise ratio (SNR), as described in our previous work [13]. In the case of FLASH-RT, the dose per pulse is on the order of 20 cGy, leading to an acoustic pressure on the order of 4 Pa. This pressure level is well above the detectable pressure by current commercially available transducers, and hence eliminates the need for high gain signal amplification and extensive signal averaging as in CONV-RT applications. Depending on the level of the iRAI signals generated, the dynamic range of

the acquisition system can be adjusted to utilize the full range while preventing signal saturation. This unique capability for single-pulse dosimetry with iRAI constitutes much of the motivation for this work.

Dosimetry Nomenclature

Typically, in CONV-RT, the dose rate that is reported is the average dose rate, D_r, which is the dose deposited over a specified time frame (i.e., Gy/min or Gy/s). Additionally, dose rate can be defined as the rate at which the dose is deposited over a single linac pulse, this is known as the instantaneous dose rate, $\dot{D}_r$ (Gy/s). With FLASH-RT using a pulsed delivery system, such as a linac, it is useful to consider the amount of dose that is deposited from a single pulse, D_p, (Gy/pulse) since the full prescribed dose can be delivered over a handful of pulses. In this work, iRAI signal amplitudes are compared to D_p, the delivered dose per pulse.

FLASH Electron Source

A Varian Clinac 2100EX (Varian Medical Systems, Palo Alto, Ca) linear accelerator (linac) was used to assess iRAI for real-time dosimetric imaging with electron beams at FLASH-RT level dose rates. All modifications were done during the decommissioning of this linac machine. In order to achieve FLASH dose rates (> 40 Gy/s), the linac was operated in 6 MV photon mode (which, typically, has the highest electron current compared with other modes) with the target and the flattening filter removed. The target is made to retract in 6MV mode by reversing the wiring to the gantry air manifold, which activates the solenoids for positioning the target for low energy X-ray mode vs electron mode. Prior to the target removal, the electron current at the target was measured through the "Target" BNC connector on the control panel to be 100 mA. The monitor chamber functioned as a scattering foil, spreading out the electron beam.

The objective of this configuration was to achieve flash dose rates at the nominal linac gantry isocenter, for this linac at 100 cm source-axis distance (SAD). This configuration was different from previous work in the literature, which focused on reversible linac modifications where the linac was running in electron mode (smaller electron current) and measurements took place within the linac head [22, 23]. The method chosen for this study removed the previous constraint of limited space within the linac head, allowing for flexibility in experimental designs for iRAI in this proof-of-concept study. However, the major downside of this modification is that it is currently irreversible. Therefore, the FLASH modifications were only made after the linac was no longer needed for clinical care.

The beam was controlled using an Arduino Uno microcontroller that was connected to the beam hold card. This allowed control of the time that the beam was turned on to be as low as 1 millisecond. The desired beam run time was entered using a keypad (as shown schematically in Figure 1) that was programmed into

the Arduino. During beam delivery with service mode, the beam would be turned on and the Arduino would maintain this beam hold until the trigger, releasing the beam for the desired time.

Fig. 1. A schematic and a photo of the Arduino-based control system which is connected to the Linac beam-hold card to control the time the beam is turned ON.

Film Dosimetry

Dose was measured using GAFChromic EBT-XD dosimetry film (Ashland Advanced Materials), which was scanned using an Expression 10000XL (Epson) flatbed scanner at a resolution of 72 dpi. All films were analyzed using the FilmQA Pro 2016 software (Ashland Advanced Materials) with the dose map being generated using the built-in triple channel uniformity optimization algorithm. Dose was determined from an average of a 0.2 cm × 0.2 cm region of interest at the central axis of the beam. Calibration was done using a 10 cm × 10 cm field of 6MV photons at reference conditions, where the film was placed at 100 cm source-to-axis distance (SAD) with 10 cm of Solid Water (Sun Nuclear Corporation) placed on top with a calibration range of 0 to 50.51 Gy. The dose per pulse was determined by dividing the measured dose from film during a specified timeframe by the known number of pulses acquired during the same period.

Linac Pulse Monitoring

For this study, individual linac pulses were used as acquisition trigger signals for iRAI. This was accomplished by measuring the Cerenkov Emission (CE) generated in a water/glycerin solution using a silicon avalanche photodiode (Thorlabs APD101A) during each single pulse [24]. The container holding the solution was wrapped in light-blocking masking tape (Thorlabs, T743) to prevent photodetector saturation due to ambient lights. This device was placed before the electron beam was collimated and was out of the central axis of the beam, relying off scattered electrons to generate the CE during the time period when the beam was ON. The signal from the avalanche diode was carried over a 15-meter BNC cable (50 ohm) from the treatment room to the linac control room and was amplified (Olympus, 5072PR) and sent to a delay generator (Stanford Research Systems, DG535) to generate a perfect square pulse, which then went through a splitter, one signal to an analogue pulse counter (Tennelec, TC 532) and the other to the trigger input of the iRAI acquisition systems, as shown in the schematic in Figure 2.

Fig. 2. Schematic of the system setup for IRAI dosimetric measurement including the linac, the trigger system (Avalanche Photodiode, Pulse/Receiver, and Delay Generator), and the iRAI system (Transducer, Pre-Amp, and DAQ system).

iRAI Dose Measurements

To investigate the linearity of the iRAI signal amplitude with the dose delivered in each linac pulse, the dose per pulse was varied and compared with the resultant iRAI signal amplitude. Since the electron beam was diverging, the dose per pulse was changed by varying the distance between the beam source (defined where the linac bremsstrahlung target would have been if it were in place) and the transducer scanning plane, which was referred to as the source-axis distance (SAD), as shown in Figure 2. The SAD range was 100-210 cm with a step size of 10 cm. The dose sensitivity and accuracy were further evaluated by adjusting the SAD from 102 cm to 104 cm with a finer increment size of 0.5 cm. At each SAD position, the iRAI acoustic signal was measured and was repeated 30 times for further statistical analysis.

A custom-built collimator made from water equivalent plastic (Solid Water, Gammex) was placed in front of the phantom to shape the incident electron beam down to a 1×1 cm^2 field. A cylindrical phantom (diameter of 100 mm) made of porcine gelatin (10 g/100 ml, G2500, Sigma-Aldrich) was used to generate the iRAI signals. The ultrasound transducer was a cylindrically focused immersion transducer (12550 1001, Imasonic) with a central frequency of 0.5 MHz and a 6 dB bandwidth of 60%. The transducer was placed on the cylindrical surface of the phantom and coupled with ultrasound gel. This selection was based on previous experimental work [14].

The iRAI acoustic wave generated from the irradiated area within the phantom propagated through the phantom and was detected by the ultrasound transducer. The detected iRAI signal was amplified by a preamplifier (5660B, Olympus-NDT) with a 40 dB gain before going to the data acquisition (DAQ) system, which is placed outside of the treatment room. The DAQ system included a 14-bit digitizer card (Razor 14, GaGe) with a sampling rate of 10 MHz. Data acquisition was triggered using the Linac Pulse Monitoring system described above (Figure 2).

Film was used as a standard dosimetric device to correlate iRAI signal amplitudes with the generated dose per pulse, D_p. At the same SAD positions as the iRAI measurements, film measurements were performed with 150 milliseconds of electron beam illumination (controlled using the Arduino card) with the number of linac pulses counted using an analogue pulse counter. The film was placed in between two pieces of solid water. The side facing the collimator was 1 cm thick (for dose build-up) and the other piece of solid water on the film side facing away from the collimator was 2 cm thick (for backscatter and mechanical support).

Depth-dependent Dose Measurements

To measure how the deposited dose changes with tissue depth (defined as a percentage depth dose [PDD] curve) during FLASH-RT, a special phantom consisting of porcine gelatin and water fixed in a water tank was used. As shown in Figure 3, the transducer was immersed in water on one side of the tank for acoustic coupling during the scanning process. The other side of the tank was made of porcine gelatin with 10 cm removed from the front to get a sharp front edge while also allowing the center of the transducer to be aligned with this front edge of the gelatin. To minimize any additional scattering of the electron beam, the wall of the water tank along the beam path was removed. The solid water collimator (1 cm × 1 cm) was placed at the surface of the water tank and the collimated electron beam travelled through 10 cm of air before hitting the front edge of the gelatin phantom. The initial position of the transducer was where the center of the transducer focal plane aligned with the front edge of the phantom. The distance between the center of the electron beam and the detection surface of the transducer was 11.2 cm (the focal length of the focused transducer). The transducer was fixed to a motorized translation stage using optical rods (Low-Profile Motorized Translation Stage, MTS50-Z8, Thorlabs) to allow the focus of the transducer to be scanned along the electron beam path through the phantom (as denoted by the blue arrow in Figure 3) for a distance of 30 mm with a step size of 2 mm. The iRAI acoustic signal was measured 30 times at each position for statistical evaluation. Film measurements were setup using a custom 3D printed Gafchromic film holder with the distance of 2 mm between each piece of film. The first position of the film (on the surface of the custom holder) was the same as the front edge of the gelatin phantom. The gaps between each adjacent films were filled with water to achieve similar radiation attenuation as porcine gel. To accumulate a sufficient dose for film analysis, 500 milliseconds (150 pulses) of irradiation time was used.

Fig. 3. The system setup for depth-dependent dose measurement. (A) Schematic of the system setup; (B) Photograph of the system setup.

In the previous section, we outlined how the relationship between the deposited dose and iRAI amplitude was measured in a gelatin phantom using film dosimetry. This relationship can be used as part of the calibration process between the measured iRAI amplitude and the deposited dose (in gelatin). During those measurements, the depth at which the transducer was sampling the iRAI amplitude within the gelatin phantom was held constant as the dose rate was varied. During the depth dependent dose measurements, however, the transducer was repositioned to sample various depths within the gelatin phantom. Therefore, a correction factor is needed to take into account the relative electron energy and fluence changes with

respect to the calibration conditions (i.e., to recover what the measurement would have been at the conditions where the relationship between the iRAI amplitude and dose was measured). Consider the following relationship,

$$D_{iRAI}(a) = f(a) \tag{9}$$

where the iRAI dose, $D_{iRAI}(a)$, is related to the fitted function used for calibration, $f(a)$, where "a" is the iRAI signal amplitude. This relationship only holds true if the phantom material is constant (in this case gelatin) and the measurement location within the phantom is the same as what was used for the iRAI dose measurements previously described. Thus, a depth-dependent correction factor, $\gamma(z)$, is used to take into account measurement parameter changes as follows:

$$D_{iRAI}(a, z) = f(a) \cdot \gamma(z) \tag{10}$$

Dose is a function of two parameters for electrons: the stopping power, $\left(\frac{S}{\rho}\right)$, and the fluence, ϕ, as shown in Eq. (1).

Hence, the correction factor itself consists of two components, one taking into account the relative electron stopping power with depth z , $C_{\left(\frac{S}{\rho}\right)}(z)$, and the other taking into account the relative fluence changes, $C_{\phi}(z)$, which are derived in the following:

$$\gamma(z) = C_{\left(\frac{S}{\rho}\right)}(z) \cdot C_{\phi}(z) \tag{11}$$

Stopping power is electron energy dependent, as electrons transverse the phantom their energies change as a function of depth. Here, we estimate the energy change using the following equation [25], where the practical length, R_p, is estimated to be 3 cm for an electron beam with a nominal energy, E_0, of 6 MeV.

$$\bar{E}(z)E_0\left(1 - \frac{z}{R_p}\right) \tag{12}$$

The stopping powers at each depth measurement point are determined using the energies provided from the expression above and looked up using NIST tables (using the values for water). The correction factor, $C_{\left(\frac{S}{\rho}\right)}(z)$, is a ratio of the stopping power at each measurement point and the stopping power at the measurement point used in the calibration:

$$C_{\left(\frac{S}{\rho}\right)}(z) = \frac{\left(S/\rho\right)_z}{\left(S/\rho\right)_0} \tag{13}$$

In order to take into account the change in fluence with respect to the calibration condition, a Monte Carlo simulation (EGSnrc) is used to determine fluence values as a function of depth for a respective material, which in this case is gelatin. The correction factor for relative fluence changes, $C_\phi(z)$, is the ratio between the fluence at each depth and the fluence at the calibration measurement point:

$$C_\phi(z) = \frac{\phi(z)}{\phi_0} \tag{14}$$

Real-time Dual Modality Imaging for Dose Mapping

A cylindrical porcine gelatin phantom (diameter = 100 mm) with a whole rabbit liver embedded was used to evaluate the feasibility of real-time single pulse dose mapping with respect to soft tissue anatomy. This was achieved using a clinically-ready integrated dual-modality imaging system that was adapted from a commercially available research ultrasound (US) platform (Verasonics, Vantage 256). This system was used in this study for both iRAI and B-mode US imaging. With 256 parallel channels, two phased array probes (Philips P4-1, 1-4 MHz, 96 elements) were driven by this system simultaneously. The two probes were oriented orthogonally (90-degree angle) with both probes facing the center of the sample (as shown on the right in Figure 4). The sample which was subsequently irradiated with electrons from the top with a solid water collimator above the sample to shape the beam to a 1 cm × 1 cm square (as shown in Figure 4). The transducer scan plane was 100 cm SAD where a dose rate of 25 cGy per pulse was achieved.

The triggers from the delay generator of the linac pulse monitoring system were sent to the dual-modality imaging system for synchronization. The iRAI signals from each linac pulse were acquired by the imaging system with IRAI images reconstructed and displayed in real time. For US B-mode, the probes were driven by the Verasonics system which displayed the B-mode images every 6 trigger events (linac pulses) for tracking continuous tissue motion. The current dual imaging system can operate in the iRAI mode and the US mode alternatively, as described in previous work [18]. Briefly, during the "beam ON" portion of the irradiation duty cycle, the transducers measured the iRAI signals in a receive-only mode; while during the "beam OFF" portion, the same transducers were used to generate a B-mode US image. The two iRAI images acquired by the two probes were compounded. The same step was performed for the two US images. Then, registration was accomplished by overlaying the resultant iRAI image on the US B-mode image. Both the probes and phantom were immersed in water for ultrasound coupling. To mimic the organ motion, the phantom was driven by a motorized stage (Low-Profile Motorized Translation Stage, MTS50-Z8, Thorlabs)

moving in the direction along the green arrow, as shown in Figure 4, at a velocity of 3 mm/s. Over a time period of 16.7 seconds, the sample moved a total distance of 50 mm.

Fig. 4. The system setup for real-time dual modality imaging for dose mapping. (A) Schematic of the system setup. (B) The photograph of the system setup.

Results

Linearity of iRAI Dosimetric Measurement

Fig. 5. Comparison of iRAI dose measurement and film measurement. (A) The iRAI dose measurement compared with film measurement along with different SAD; (B) The linearity of iRAI dosimetric measurement.

Figure 5(A) presents the detected iRAI signal amplitude as a function of SAD compared with film dosimetry. The boxplot consists of 30 measurements at each SAD, demonstrating the high stability of iRAI for dosimetric measurements. The film measurements show that the dose per pulse decreases with increasing SAD, ranging from 24.5 cGy/pulse at 100 cm SAD to 1.4 cGy/pulse at 210 cm SAD. iRAI amplitude measurements followed the same decreasing trend with a root mean square error (RSME) of 0.00073. When plotting the iRAI signal amplitude versus the film measured dose per pulse, D_p, as shown in Figure 5(B), a linear relationship is found with an r^2 value of 0.9998, demonstrating high linearity for iRAI dosimetric measurements. The fitting line with proportionality factor of 0.0047 is consistent with the theory of iRAI dosimetric measurement described in Eq. (7).

Dose Sensitivity of iRAI Dosimetric Measurements

For this set of measurements, the SAD step size was reduced to 0.5 cm to assess the dose sensitivity of iRAI. Figure 6 compares both the measured iRAI signal amplitude and the normalized dose per pulse derived from film dosimetry as a function of SAD. A dose fitting line based on the attenuation equation (inverse square law) of electron beam in air was extracted with the data of the linearity measurement shown in Figure 5(A). Although the slope of the film measurement and the calculated dose as a function of SAD is the same, the film measurement shows some offsets in some SADs. With the iRAI measurements drawn

with black error bars, the average value at each SAD of the iRAI measurements is more consistent with the calculated dose than the film measurement. Unlike the film measurement at each SAD which reflects the dose accumulated in 150 milliseconds with 45 pulses, the iRAI measurements at each SAD gives the dose of 30 individual pulses. The maximum standard deviation of the iRAI based single pulse dose measurements over the five SAD positions is within 1% with an average dose difference between the SAD steps less than 2.5%.

Fig. 6. The quantified sensitivity and accuracy of iRAI dose measurement.

Depth-dependent Dose Measurements

Fig. 7. Comparison of iRAI and film dose measurements as a function of depth. The black curve is the normalized film measurement, while the blue curve and the red curve are the uncorrected and the corrected normalized iRAI measurements, respectively.

Figure 7 compares the normalized depth-dependent dose measurements from iRAI with those from the film dosimetry. The curve showing the iRAI measured dose .vs. depth (blue curve) shows similar and expected features as the measurement from the film (black curve), such as a dose buildup region, a maximum dose point, and a fall off region. The iRAI voltage vs dose relationship (Figure 5) was used as a calibration curve for dose measurement. In order to account for the departure of the calibration conditions in Figure 5, a correction factor was introduced that compensated for the electron beam divergence and its energy changes as a function of phantom depth using Monte Carlo simulated fluence changes, as described by Eq. (9)-(14). The iRAI measurement of the PDD after applying this correction factor, as shown by the red curve in Figure 5, improved agreement with the measurements from the film. Using the film measurements as the gold standard, the RSME of the iRAI measurements was improved from 0.3774 (uncorrected) to 0.0243 (corrected) by applying this correction factor.

Real-Time Dual Modality Imaging for Dose Mapping

The iRAI and US dual-modality imaging results from the rabbit liver phantom are shown in Figure 8. Figure 8(A) shows a registered and combined iRAI and US image. The iRAI image and the US image each was acquired by using both of the two orthogonally oriented probes shown in Figure 4(B). The pseudo-

color iRAI image shows the boundary of the dose distribution in red. This illustrates that our transducer's frequency bandwidth is primarily sensitive to the boundary of the dose deposition from this large treatment field. The position of the delivered high dose rate electron beam is marked by the yellow dashed box, which corresponded well with the iRAI image. During a time period of 16.7 seconds, the rabbit liver phantom was translated in one direction (using the motor drive) during constant irradiation, with both the beam and transducer positions fixed. With the multi-frame image shown in Figure 8(B), the relative dose position in the phantom as a function of time is mapped successfully. The signal-to-noise ratio (SNR) of iRAI working with the high dose rates during FLASH-RT is high enough to allow for imaging with single linac pulses. Hence, iRAI based imaging of the radiation beam location in the soft-tissue samples can work at a frame rate of 300 Hz (i.e., the linac repetition rate). The video of this dual-modality imaging result from the ex vivo rabbit liver phantom, as shown in supplemental material (Movie S1), has a frame rate of 50 Hz, since the B-mode US images were acquired after every six linac pulses.

Fig. 8. IRAI and US dual-modality imaging of a rabbit liver phantom ex vivo. (A) A registered and combined IRAI and US image. (B) The multi-frame combined images from real-time IRAI and US dual-modality imaging at different time points when the phantom was translated.

Discussion

Compared with CONV-RT, where the prescribed radiation dose is delivered using hundreds to thousands of linac pulses over several minutes, FLASH-RT can deliver the same dose in a fraction of a second using only a handful of high dose linac pulses, leading to a transient oxygen depletion effect. This phenomenon has been demonstrated to be an essential feature for sparing normal tissue while maintaining the same efficacy in eradicating tumors, leading to approximately a 20-30% reported reduction in toxicity in preclinical studies [2-9]. However, the translation of FLASH-RT into clinical practice would require addressing many new implementation challenges, such as precise pulse-to-pulse dosimetry and precise beam targeting when delivering such high dose pulses. Additionally, knowing what the dose deposition at depth within tissue and with respect to anatomy would allow for real-time measurements to identify any regions where the dose rates may deviate, i.e., fall above or below the FLASH-RT threshold, which can inadvertently lead to severe normal tissue complications or failed treatment with even possible death.

The goal of this study is to investigate the feasibility of iRAI for real-time deep tissue dosimetry with single linac pulse resolution as well as co-registration of the delivered dose to exposed soft tissue anatomy during FLASH-RT. For this proof-of-concept study, a modified clinical linac is used to deliver 6 MeV electrons at FLASH dose rates at isocenter. Two measurement setups are used, one based on a single element cylindrically focused transducer for point measurements and the other based on an iRAI and B-mode US dual-modality system built on a commercial US unit and phase arrays.

Using a single element transducer, the iRAI amplitude is compared with standard film dosimetry. Intrinsically, the iRAI signal is the result of a single linac pulse and is thus proportional to the delivered dose per pulse, D_p. In order to correlate the iRAI signal with the film result, the D_p is first derived from the film measurements, which is done by dividing the dose measured by the film by the measured number of pulses delivered. When compared to the film result, the iRAI signal amplitude exhibits high linearity (r^2 = 0.9998) with D_p, thus demonstrating the feasibility of iRAI for use as a dosimeter. Additionally, the experiments conducted for measuring the accuracy and uncertainty of iRAI measurement shows the average dose difference between each SAD increment to be about 2.5%. The statistical significance between the iRAI measurements at different SADs demonstrates that the dose resolution of this method is smaller than 2.5%. By calculating the standard deviation of the iRAI signal amplitudes at each SAD, a maximum standard deviation of 1% is determined which demonstrates the reproducibility uncertainty of iRAI dosimetric measurement in the homogenous phantom. It is worth noting that in an in vivo system, this uncertainty is likely to higher, partly due to the differences in various tissue properties affecting the radiation-induced thermoacoustic effect. However, the use of the dual iRAI/US imaging system may help mitigate this issue [18].

By normalizing the theoretical dose which was fitted using the linearity measurement and the dose measurement at each specific position, the correlation between the average values of the iRAI measurements and the theoretical doses is higher than the correlation between the film measurements and the theoretical doses. Since the film measurement is the average dose integrated over a time period with more than a hundred single pulses, the variation between the film measurements and the theoretical doses is within the uncertainty of the iRAI measurements.

This work also demonstrates the potential of using iRAI for deep tissue dosimetry. A typical measurement in clinical quality assurance is the PDD curve where dose is measured as a function of depth (which is typically done using an ionization chamber in a water tank). To assess the feasibility of using iRAI to measure dose at depth, the single element transducer is used to sample the generated acoustic signal at various depths. For comparison, dose is also measured with film placed at various depths in water. Film is chosen over using an ionization chamber due to recombination saturation during the ultra-high dose rates

of FLASH-RT. As shown in Figure 5, the measurement depth for the irradiated beam is kept consistent between the iRAI and the film measurement, including the 10 cm distance between the collimator and the surface of the phantom. As electrons travel in the phantom, their spatial distribution spreads out following a teardrop shape and their average energy decreases [25]. In order to correctly apply the iRAI voltage vs dose relationship as a function of depth, a correction factor must be used to compensate the departure from the fixed measurement condition. This correction factor is generated using a Monte Carlo simulation (EGSnrc) of electron transport in medium. It takes into account the relative energy changing with depth as well as relative fluence changes (with respect to the calibration conditions) as the beam spreads out to account for deviations in measurement conditions compared to the calibration conditions at a fixed depth. When applying the corrections, the iRAI measured dose depth curve is in closer agreement with the film results. Both the iRAI and the film show a buildup region, a maximum, and a fall off region in the depth dose curve. In the buildup region near the surface, the film measurements had a higher signal. This is due to how the signal is collected with iRAI. The focal zone of the transducer is not a point source but a finite volume, thus is unable to collect the signal from a single plane with an infinitesimal thickness. When taking measurements at the surface, some of the beam in the focal zone extends out of the phantom, sacrificing part of the acoustic propagation, thereby reducing the signal amplitude, which is consistent with the measurements shown in Figure 7. The dose depth measurements using the film and the IRAI show excellent agreement in the fall off region. When looking at the detection limit of the film measurement in Figure 7 at the depth of 26 mm, iRAI can still detect a relatively strong acoustical signal. Compared with the film measurement, the standard deviation of the iRAI signals at each depth are dominated by pulse-to-pulse measurement fluctuation (which may result from both the stability of data acquisition system as well as the actual linac pulse-to-pulse variations), while the film measurement has an average of 150 linac pulses delivered over the irradiation time of 500 milliseconds. When considering these uncertainties, the iRAI derived PDD measurements are consistent with the film measurements. For direct dose measurements on patients, no current clinical dosimetry method exists for such deep tissue dosimetry with current methods limited to superficial measurements as noted earlier. It is worth noting that in future practice, single element iRAI depth dose measurements will be substituted in lieu of the use of 1D or 2D phased array transducers to acquire a full 2D/3D images for accurate spatial dose distribution measurements.

Using the iRAI and US dual-modality system, the ability to map the deposited dose with respect to tissue anatomy in real time is demonstrated using an ex vivo rabbit liver phantom. Figure 8 shows the boundary of the radiation field location within the rabbit liver. By taking advantage of the high SNR from the high dose per pulse in FLASH-RT and the large number of parallel channels in the research US platform, the dose mapping of the radiation beam and anatomical information from B-mode ultrasound can be achieved with a single radiation pulse in real-time. Intrinsically, the iRAI and US images are co-registered since the

same probes are used. It is worth noting here that the dose map generated is based upon a relative measurement that demonstrates the ability for beam co-localization but does not provide an absolute dose measurement. It is difficult to quantify the exact dose being deposited since various tissue types are different in an array of parameters affecting the radiation-induced thermoacoustic effect. For example, an anatomical feature consisting of mostly fat with larger Grüneisen parameter would have a larger iRAI amplitude than surrounding soft tissue being irradiated with the same dose. This means that a simple calibration using the approximation of a water-based phantom (as used for the single element transducer studies) may not be appropriate. Future work will require iRAI measurements to take the varying tissue properties, possibly using the dual US imaging as presented here with further segmentation analysis of the B-mode image to characterize the different tissue types in order to provide an accurate absolute dose measurement.

To further advance this technique for clinical translation, studies on in vivo models as well as more sophisticated iRAI reconstruction algorithms that take into account tissue inhomogeneity for absolute dosimetry are needed. Despite these limitations, the current results from the two prototype iRAI systems and the proof-of-concept experiments on the soft tissue phantoms demonstrate the feasibility and accuracy of iRAI for real-time single radiation pulse deep tissue in vivo dosimetry during FLASH-RT, as well as real-time mapping of the dose deposition with respect to surrounding tissue, which in itself is an important enabling step for the safe clinical translation of FLASH-RT.

Conclusions

This work has demonstrated the potential of using iRAI for real-time deep tissue dosimetry for FLASH-RT. It is shown that iRAI signals are linear ($r^2 = 0.9998$) with dose. In addition, when combined with US imaging, iRAI can map radiation dose with respect to local soft tissue anatomy. With its ability to measure dose for individual linac pulses at any location within soft tissue while knowing where that dose is being delivered anatomically in real time, iRAI can be a powerful tool to enable safe and successful clinical translation of FLASH-RT.

Acknowledgements

The authors would like to thank Dr. Peter Balter from MD Andersen for his help with the Arduino card configuration. Part of this work was supported by NIH grant R37-CA222215.

Conflict of Interest

The authors have no relevant conflict of interest to disclose.

References

1. Ezzell, G.A., J.M. Galvin, D. Low, J.R. Palta, I. Rosen, M.B. Sharpe, P. Xia, Y. Xiao, L. Xing, and C.X. Yu, Guidance document on delivery, treatment planning, and clinical implementation of IMRT: Report of the IMRT subcommittee of the AAPM radiation therapy committee. Medical Physics, 2003. **30**(8): p. 2089-2115..
2. Montay-Gruel, P., M.M. Acharya, K. Petersson, L. Alikhani, C. Yakkala, B.D. Allen, J. Ollivier, B. Petit, P.G. Jorge, A.R. Syage, T.A. Nguyen, A.D. Baddour, C. Lu, P. Singh, R. Moeckli, F. Bochud, J.F. Germond, P. Froidevaux, C. Bailat, J. Bourhis, M.C. Vozenin, and C.L. Limoli, Long-term neurocognitive benefits of FLASH radiotherapy driven by reduced reactive oxygen species. Proceedings of the National Academy of Sciences of the United States of America, 2019. **116**(22): p. 10943-10951.
3. Simmons, D.A., F.M. Lartey, E. Schüler, M. Rafat, G. King, A. Kim, R. Ko, S. Semaan, S. Gonzalez, M. Jenkins, P. Pradhan, Z. Shih, J. Wang, R. von Eyben, E.E. Graves, P.G. Maxim, F.M. Longo, and B.W. Loo, Jr., Reduced cognitive deficits after FLASH irradiation of whole mouse brain are associated with less hippocampal dendritic spine loss and neuroinflammation. Radiotherapy and Oncology, 2019.
4. Montay-Gruel, P., K. Petersson, M. Jaccard, G. Boivin, J.F. Germond, B. Petit, R. Doenlen, V. Favaudon, F. Bochud, C. Bailat, J. Bourhis, and M.C. Vozenin, Irradiation in a flash: Unique sparing of memory in mice after whole brain irradiation with dose rates above 100 Gy/s. Radiotherapy and Oncology, 2017. **124**(3): p. 365-369.
5. Montay-Gruel, P., A. Bouchet, M. Jaccard, D. Patin, R. Serduc, W. Aim, K. Petersson, B. Petit, C. Bailat, J. Bourhis, E. Brauer-Krisch, and M.C. Vozenin, X-rays can trigger the FLASH effect: Ultra-high dose-rate synchrotron light source prevents normal brain injury after whole brain irradiation in mice. Radiotherapy and Oncology, 2018. **129**(3): p. 582-588.
6. Favaudon, V., L. Caplier, V. Monceau, F. Pouzoulet, M. Sayarath, C. Fouillade, M.F. Poupon, I. Brito, P. Hupe, J. Bourhis, J. Hall, J.J. Fontaine, and M.C. Vozenin, Ultrahigh dose-rate FLASH irradiation increases the differential response between normal and tumor tissue in mice. Science Translational Medicine, 2014. **6**(245).
7. Favaudon, V., C. Fouillade, and M.C. Vozenin, Ultrahigh dose-rate, "flash" irradiation minimizes the side-effects of radiotherapy. Cancer Radiotherapie, 2015. **19**(6-7): p. 526-531.
8. Vozenin, M.C., P. De Fornel, K. Petersson, V. Favaudon, M. Jaccard, J.F. Germond, B. Petit, M. Burki, G. Ferrand, D. Patin, H. Bouchaab, M. Ozsahin, F. Bochud, C. Bailat, P. Devauchelle, and

J. Bourhis, The Advantage of FLASH Radiotherapy Confirmed in Mini-pig and Cat-cancer Patients. Clinical Cancer Research, 2019. **25**(1): p. 35-42.

9. Bourhis, J., W.J. Sozzi, P.G. Jorge, O. Gaide, C. Bailat, F. Duclos, D. Patin, M. Ozsahin, F. Bochud, J.-F. Germond, R. Moeckli, and M.-C. Vozenin, Treatment of a first patient with FLASH-radiotherapy. Radiotherapy and Oncology, 2019. **139**: p. 18-22.
10. Jaccard, M., M.T. Duran, K. Petersson, J.F. Germond, P. Liger, M.C. Vozenin, J. Bourhis, F. Bochud, and C. Bailat, High dose-per-pulse electron beam dosimetry: Commissioning of the Oriatron eRT6 prototype linear accelerator for preclinical use. Medical Physics, 2018. **45**(2): p. 863-874.
11. Petersson, K., M. Jaccard, J.F. Germond, T. Buchillier, F. Bochud, J. Bourhis, M.C. Vozenin, and C. Bailat, High dose-per-pulse electron beam dosimetry - A model to correct for the ion recombination in the Advanced Markus ionization chamber. Medical Physics, 2017. **44**(3): p. 1157-1167.
12. Jaccard, M., K. Petersson, T. Buchillier, J.F. Germond, M.T. Duran, M.C. Vozenin, J. Bourhis, F.O. Bochud, and C. Bailat, High dose-per-pulse electron beam dosimetry: Usability and dose-rate independence of EBT3 Gafchromic films. Medical Physics, 2017. **44**(2): p. 725-735.
13. Lei, H., W. Zhang, I. Oraiqat, Z. Liu, J. Ni, X. Wang, and I. El Naqa, Toward in vivo dosimetry in external beam radiotherapy using x-ray acoustic computed tomography: A soft-tissue phantom study validation. Med Phys, 2018.
14. Hickling, S., H. Lei, M. Hobson, P. Léger, X. Wang, and I. El Naqa, *Experimental evaluation of x-*ray acoustic computed tomography for radiotherapy dosimetry applications. Medical physics, 2017. **44**(2): p. 608-617.
15. Xiang, L., S. Tang, M. Ahmad, and L. Xing, High Resolution X-ray-Induced Acoustic Tomography. Sci Rep, 2016. **6**: p. 26118.
16. Xiang, L., B. Han, C. Carpenter, G. Pratx, Y. Kuang, and L. Xing. X-ray induced photoacoustic tomography. in SPIE BiOS. 2013. International Society for Optics and Photonics.
17. Zhang, W., H. Lei, I. Oraiqat, I.E. Naqa, and X. Wang, Real-time monitoring the alignment of x-ray beam relative to treatment target during radiation treatment based on ultrasound and x-ray acoustic dual-modality imaging (Conference Presentation). SPIE BiOS. Vol. 10494. 2018: SPIE.
18. Zhang, W., Oraiqat, I., Lei H., Carson, P., El Naqa, I., and Wang, W., (In Press), X-ray induced radiation acoustic and ultrasound imaging for real-time monitoring of radiotherapy, BME Frontiers, 2020.

19. Hickling, S., Xiang, L., Jones, K.C., Parodi, K., Assmann, W., Avery, S., Hobson, M. and El Naqa, I. (2018)**,** *Ionizing radiation-induced acoustics for radiotherapy and diagnostic radiology* applications. Med. Phys., 45: e707-e721. doi:10.1002/mp.12929
20. Hickling, S., M. Hobson, and I. El Naqa, Feasibility of x-ray acoustic computed tomography as a tool for noninvasive volumetric in vivo dosimetry. International Journal of Radiation Oncology• Biology• Physics, 2014. **90**(1): p. S843.
21. Hayakawa, Y., Tada, J., Arai, N., Hosono, K., Sato, M., Wagai, T., Tsuji, H. and Tsujii, H., Acoustic pulse generated in a patient during treatment by pulsed proton radiation beam. Radiat. Oncol. Investig., 3: 42-45. doi:10.1002/roi.2970030107, 1995
22. Schuler, E., S. Trovati, G. King, F. Lartey, M. Rafat, M. Villegas, A.J. Praxel, B.W. Loo, and P.G. Maxim, Experimental Platform for Ultra-high Dose Rate FLASH Irradiation of Small Animals Using a Clinical Linear Accelerator. International Journal of Radiation Oncology Biology Physics, 2017. **97**(1): p. 195-203.
23. Lempart, M., B. Blad, G. Adrian, S. Bäck, T. Knöös, C. Ceberg, and K. Petersson, Modifying a clinical linear accelerator for delivery of ultra-high dose rate irradiation. Radiotherapy and Oncology, 2019.
24. Oraiqat, I., S. DeBruin, R. Pearce, C. Como, J. Mikell, C. Taylor, J. Way, M. Suarez, A. Rehemtulla, R. Clarke, and I.E. Naqa, Silicon Photomultipliers for Deep Tissue Cerenkov Emission Detection During External Beam Radiotherapy. IEEE Photonics Journal, 2019. **11**(4): p. 1-16.
25. Gerbi, B.J., J.A. Antolak, F.C. Deibel, D.S. Followill, M.G. Herman, P.D. Higgins, M.S. Huq, D.N. Mihailidis, E.D. Yorke, K.R. Hogstrom, and F.M. Khan, Recommendations for clinical electron beam dosimetry: Supplement to the recommendations of Task Group 25. Medical Physics, 2009. **36**(7): p. 3239-3279.

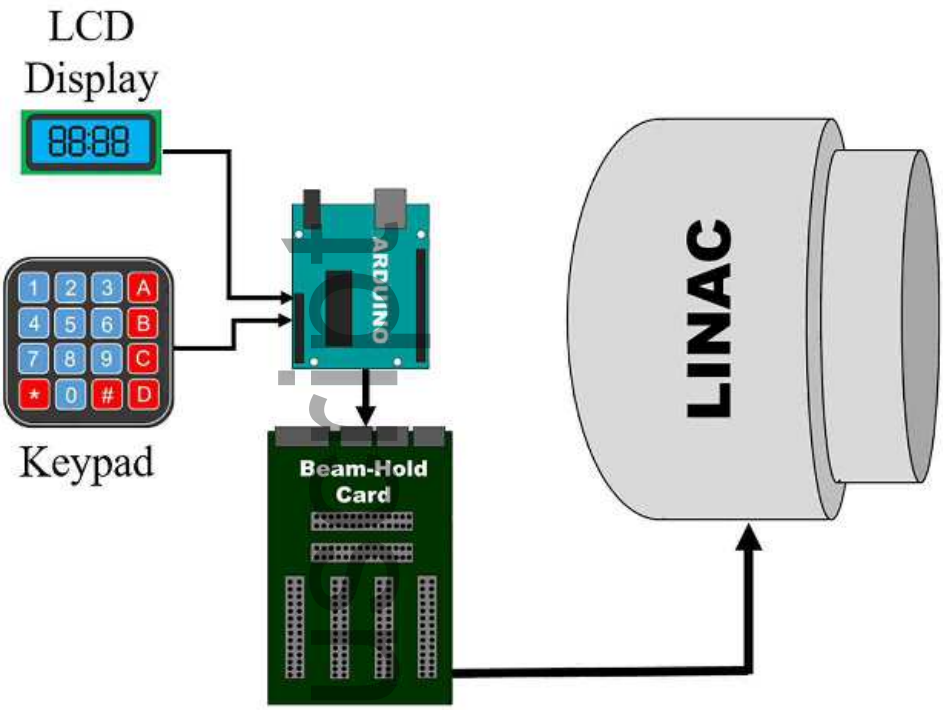

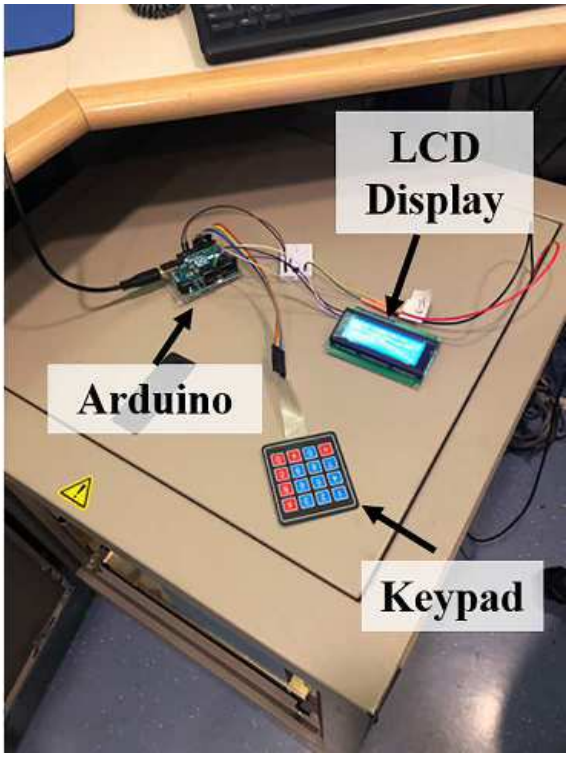

mp_14358_f1.eps

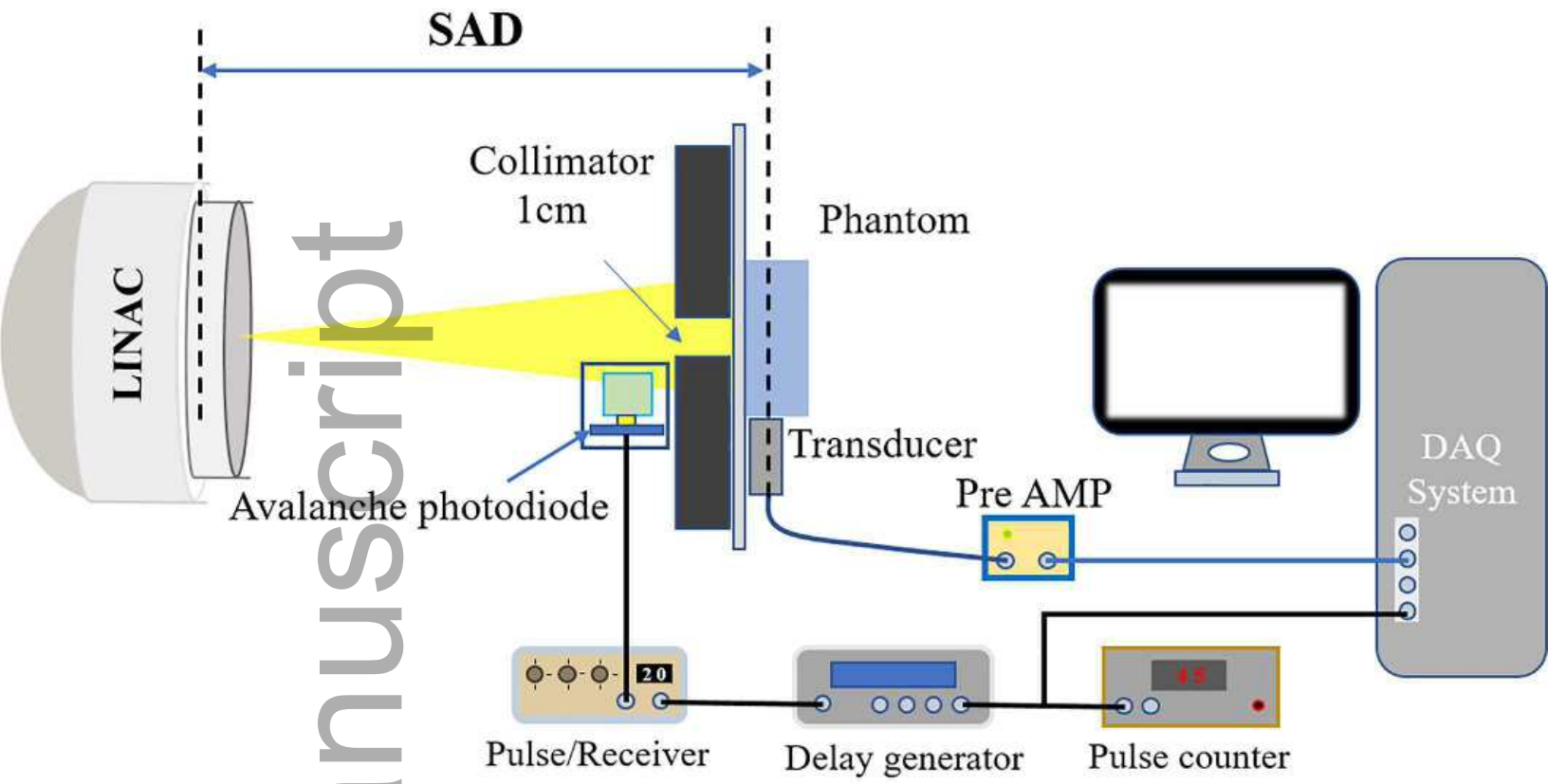

mp_14358_f2.eps

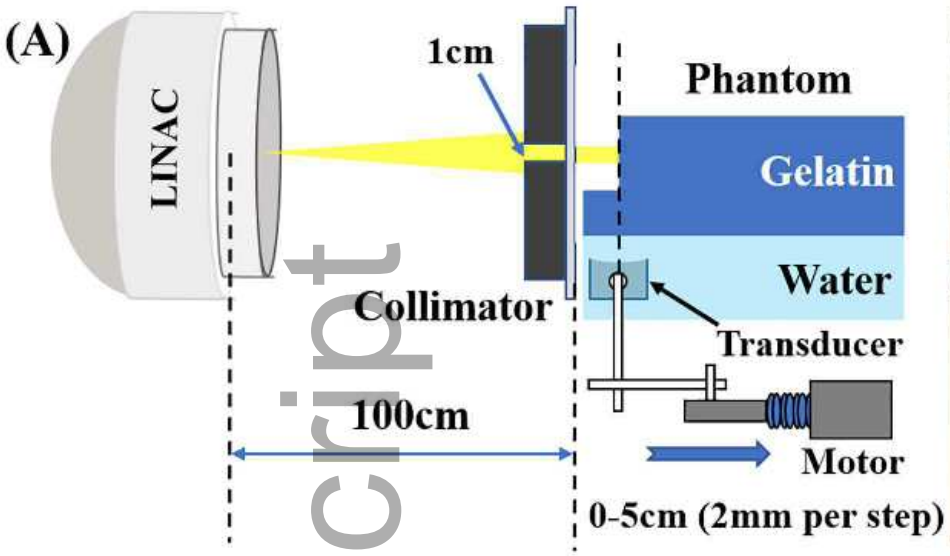

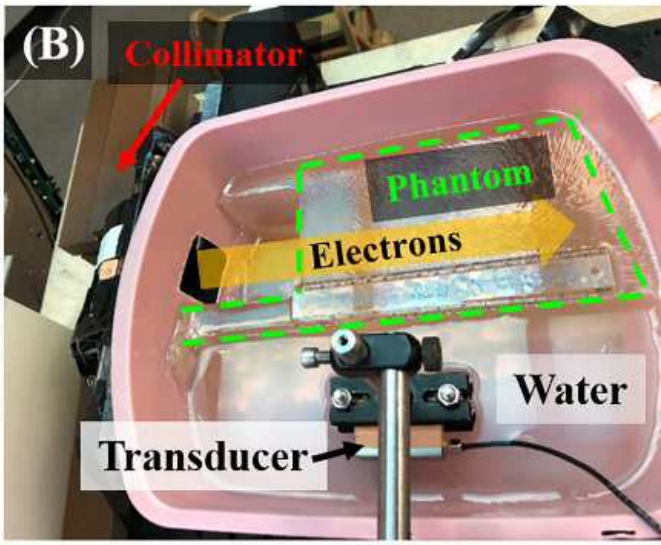

mp_14358_f3.eps

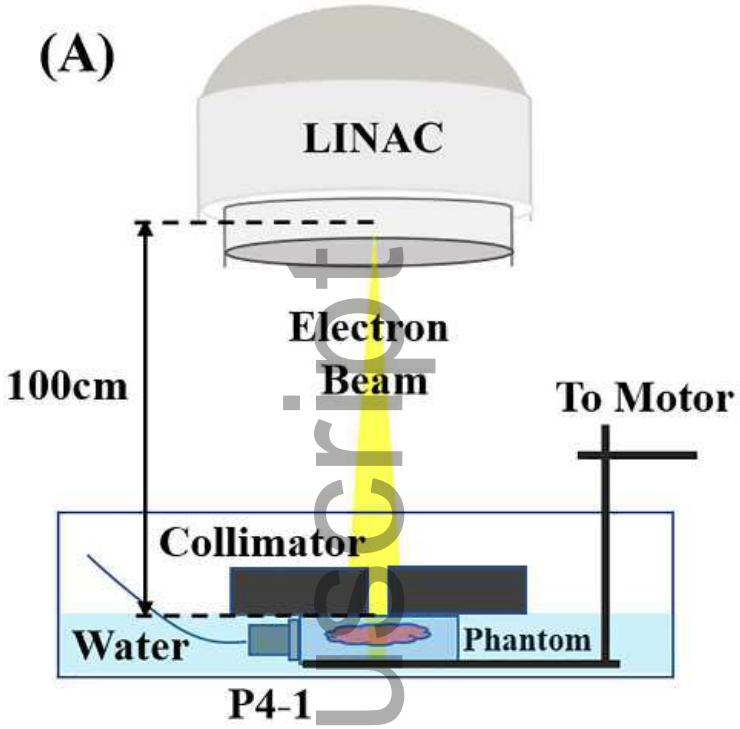

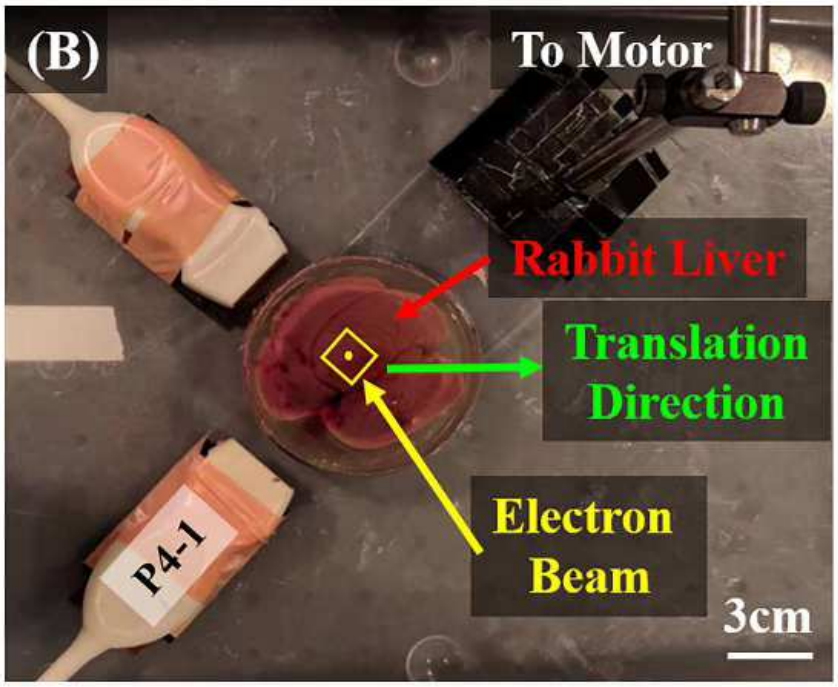

mp_14358_f4.eps

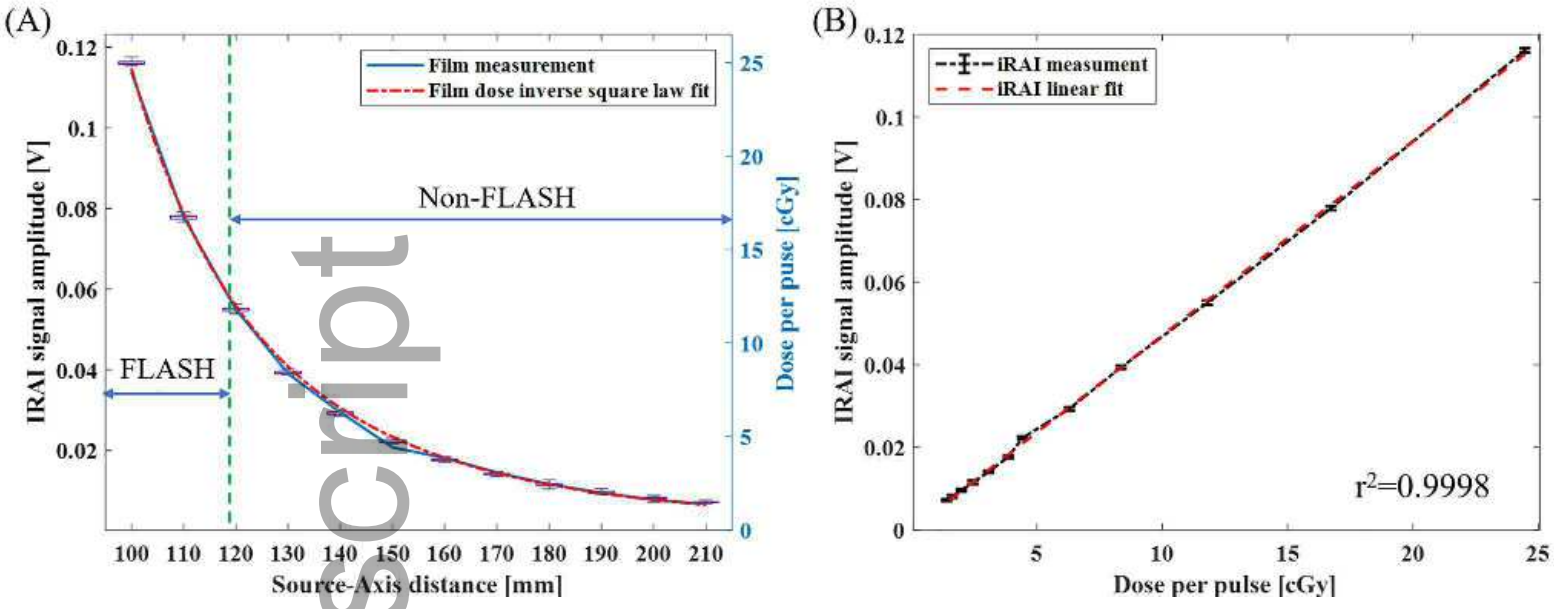

mp_14358_f5.eps

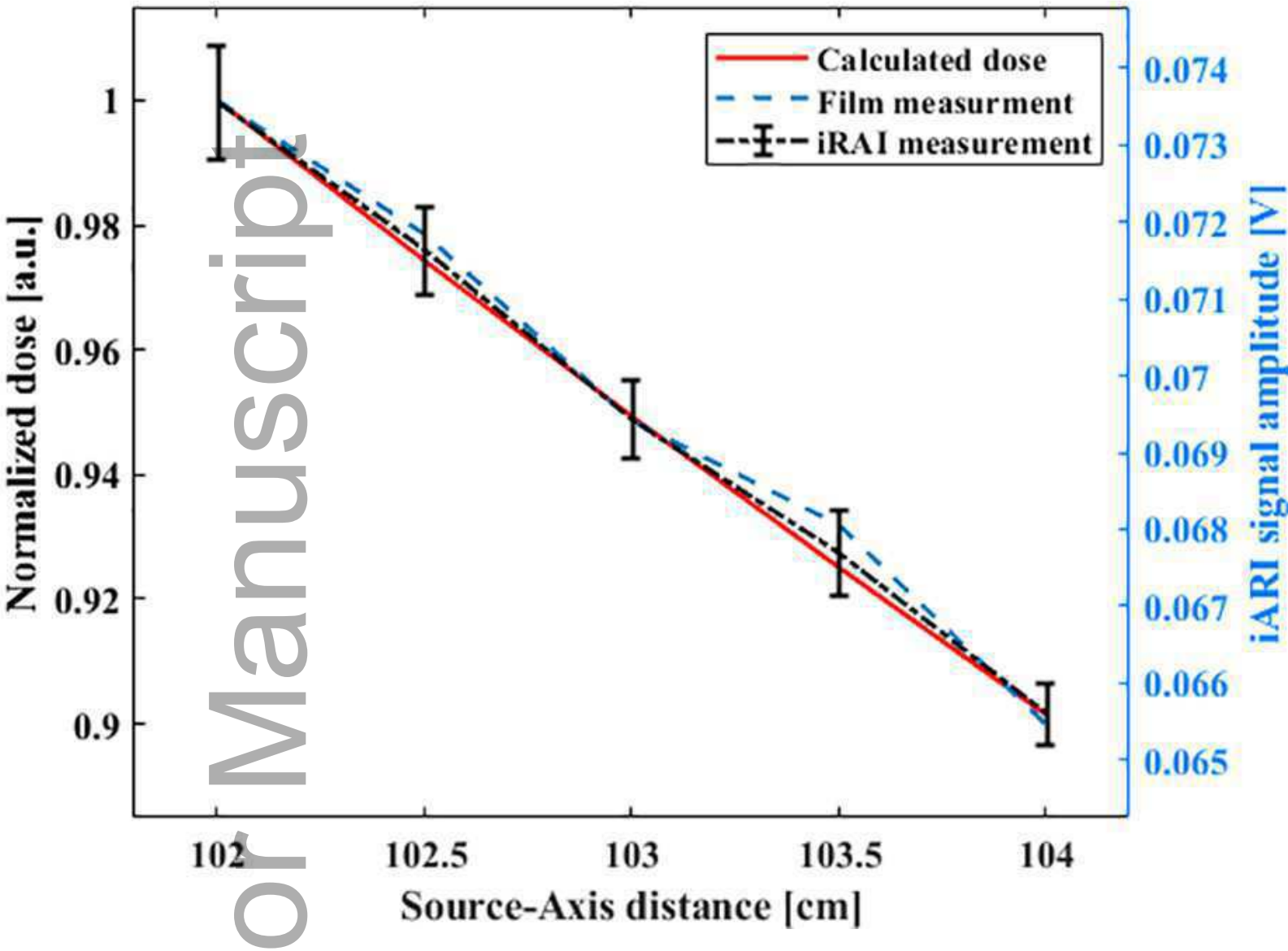

mp_14358_f6.eps

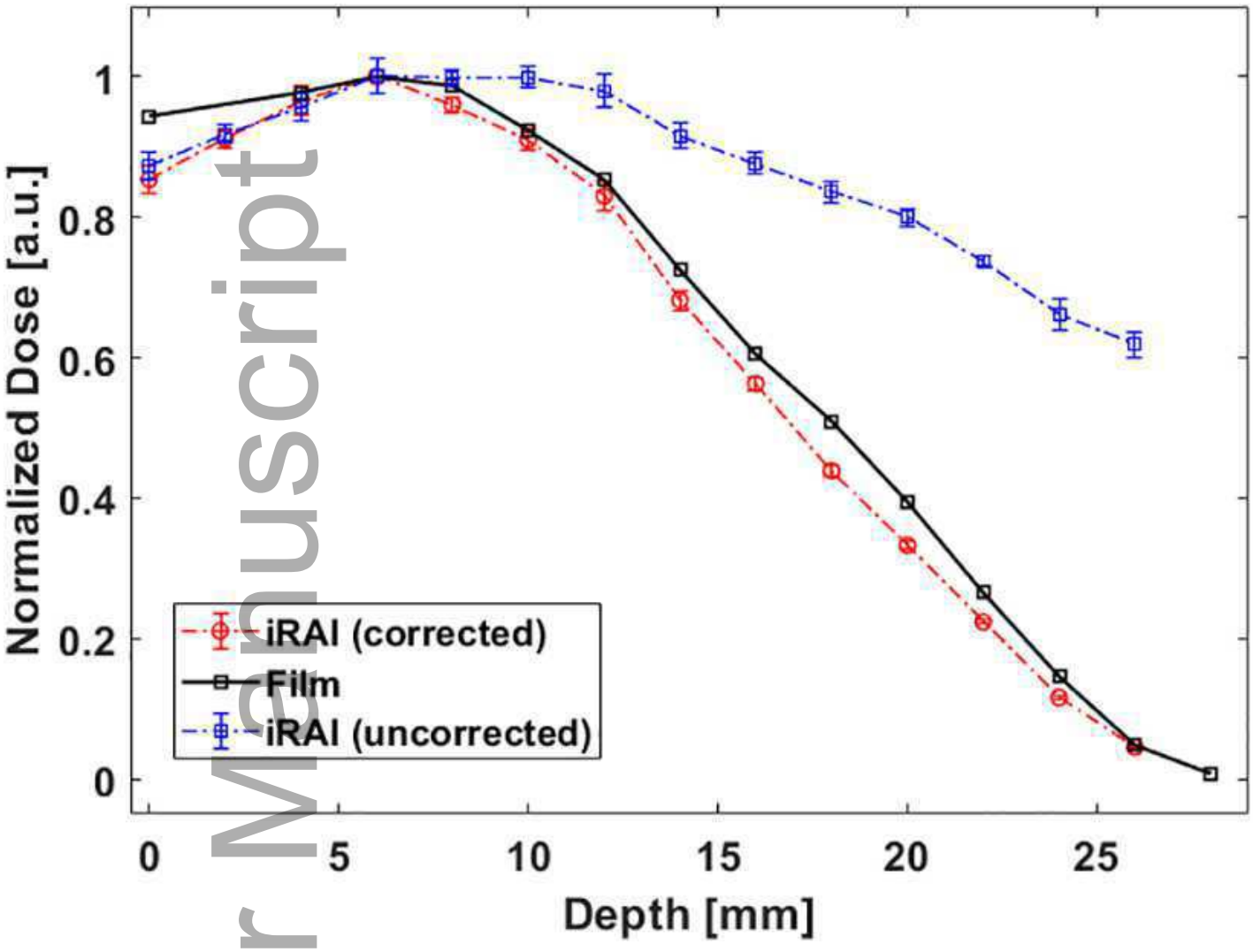

mp_14358_f7.eps

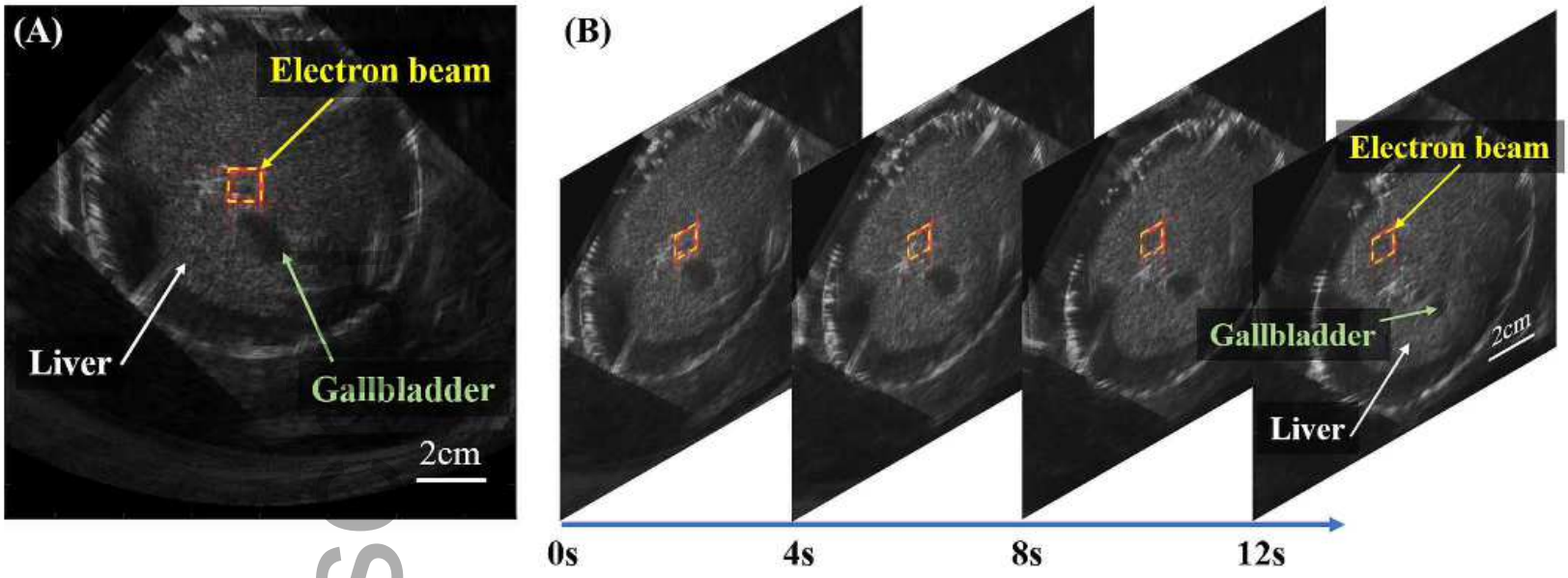

mp_14358_f8.eps